Chinese Journal of
POLYMER SCIENCE

RESEARCH ARTICLE

https://doi.org/10.1007/s10118-022-2774-5
Chinese J. Polym. Sci. **2022**, *40*, 1679–1687

Unsteady Dynamics of Vesicles in a Confined Poiseuille Flow

Dan Liu[a], Zhi-Hao Zhang[a], Rong Wang[a*], and Jing-Lei Hu[b*]

[a] *Department of Polymer Science and Engineering, State Key Laboratory of Coordination Chemistry and Collaborative Innovation Center of Chemistry for Life Sciences, Key Laboratory of High Performance Polymer Material and Technology of Ministry of Education, School of Chemistry and Chemical Engineering, Nanjing University, Nanjing 210023, China*
[b] *Kuang Yaming Honors School & Institute for Brain Sciences, Nanjing University, Nanjing 210023, China*

Electronic Supplementary Information

Abstract The dynamic behaviors of a single vesicle bounded by the cylindrical wall in a Poiseuille flow were investigated by considering different confinements and dimensionless shear rates. By observing the evolution of two adjacent particles attached to the internal and external surfaces of the spherical vesicles, we found they had the same frequency. The vorticity trajectories formed by the time-tracing of the particles on the membrane are parallel, which can be identified as the unsteady rolling motion of the membranes due to the unfixed axis. The dynamic behaviors of vesicles are associated with the confinement degree and the dimensionless shear rate. The smaller dimensionless shear rate will result in the slower frequency of the rolling by examining the velocity of the rolling. The weakened rolling motion under stronger confinements is observed by measuring the evolution of the orientation angles. The changes of revolution axes over time can be interpreted by the lateral excursion of the center of mass on the orthogonal plane of the flow.

Keywords Vesicle; Unsteady dynamics; Dissipative particle dynamics; Poiseuille flow

Citation: Liu, D.; Zhang, Z. H.; Wang, R.; Hu, J. L. Unsteady dynamics of vesicles in a confined poiseuille flow. *Chinese J. Polym. Sci.* **2022**, *40*, 1679–1687.

INTRODUCTION

The flow field system basically consists of a flow field environment and research objects such as red blood cells (RBCs), vesicles, or capsules, which are widely used in the fields of sorting cell,[1–3] cell analysis,[4,5] drug delivery.[6,7] For example, Henry *et al*. proposed an improved strategy of sorting based on deterministic lateral displacement (DLD) experimentally, which is more effective in sorting deformable RBCs by tuning different dynamic behaviors, *i.e.*, tank treading and tumbling.[8] Merola *et al*. experimentally made the technological improvement depending on determining the angles of tumbling cells which is suitable for obtaining 3D morphologies of single healthy or pathological cell under the condition of a continuous flow.[9]

There have been a number of numerical,[10–16] experimental,[17–19] and theoretical[20–23] work regarding the dynamic behaviors (steady behaviors, unsteady behaviors, *etc*.) of vesicles or shaped objects in the flow including the shear flow and Poiseuille flow. An experiment of erythrocytes at low hematocrits is designed by Goldsmith to study the dynamics of single RBC, finding deformation and the steady tumbling motion with different directions of the rotation in Poiseuille flow.[24] Furthermore, the occurrence of multiple modes of motion, such as tank-treading,[18] trembling (also called vacillating-breathing, swinging, or oscillating),[25] rolling,[26] and chaotic[27] were demonstrated in flow. The critical viscosity ratios of transition from tank treading to trembling, and eventually to tumbling were calculated.[28] The transition from rolling to tank treading was observed in the experiment.[26]

However, the studies about unsteady behaviors are rare. Keller and Skalak provided a model for theoretically predicting the motion mode, *e.g.*, unsteady tumbling in flow by considering the viscosity ratio and ellipsoidal axis ratio.[21] Noguchi and Gompper found that the vesicles in shear flow can transform from steady tank treading to unsteady tumbling motion by tuning the membrane viscosity.[11] The unsteady tumbling with a nonconstant velocity was analyzed from the dissipation in numerical work of Beaucourt.[29] Junot *et al*. experimentally proved the typology of bacteria trajectories as non-tumbling in Poiseuille flow and found the collapsing of oscillating trajectories after a rotation.[30]

Since the vesicles provide a reliable model of obtaining the physical rules in blood, there have many attempts to explore the key factors of influencing the behaviors of vesicles in flow.[12,31,32] The parameters of confinement degrees and shear rates are the crucial conditions of the flow field system, though the investigation regarding the influence of confinement is limited. They were considered in the experiment of Holme *et al*. because the confinement degree can characterize the constricted arteries caused by the atherosclerosis with respective to healthy arteries and shear-stress sensitive vesicles are promising to accomplish the targeted drug deli-

* Corresponding authors, E-mail: wangrong@nju.edu.cn (R.W.)
E-mail: hujinglei@nju.edu.cn (J.L.H.)

Received March 15, 2022; Accepted April 23, 2022; Published online July 20, 2022

© Chinese Chemical Society
Institute of Chemistry, Chinese Academy of Sciences

very.[6] The effect of confinement degrees on the inclination and velocity of membrane in tank treading motion are studied by Kaoui.[33] They found that decreasing the confinement degree can trigger the transition from tank treading to unsteady tumbling motion.[32] Abkarian *et al.* experimentally revealed the dependence of motion transition on the shear stress.[25] The confinement degrees and the shear rates influence the dynamics of steady chaotic states.[34]

Unsteady dynamic behaviors of a single vesicle in confined Poiseuille flow are complex. However, most of the existing studies focused on several basic questions, *i.e.*, steady mode of motion and their transition. Few studies focus on the unsteady behaviors, especially in terms of the rolling.

In this study, we consider the behaviors of the motion of vesicles in confined Poiseuille flow along the flow direction and its orthogonal direction, respectively. Firstly, we analyze the stable morphology regime drawn in the phase diagram of the confinement degree and the dimensionless shear rates at a certain time. We find the phase boundary of the leakage of vesicles. Then, we determine the motion as the rolling by the time-tracing of particles around the vesicle. The rolling of vesicle membrane over time presents unsteady behaviors with the characteristic of an unfixed axis. We calculate the orientation angle with respect to *x*-axis direction. Furthermore, the relative strong confinement degree is also tested. The relationship between the dimensionless shear rates and the evolution velocity is also displayed. Finally, the excursions of the center of the mass of the vesicle on the orthogonal plane of the flow (plane *yz*) are measured to reveal the reason of the occurrence of the shifting axes.

METHOD

We use the simulation method of dissipative particle dynamics (DPD) to study the dynamic behaviors of a single vesicle in confined Poiseuille flow. The DPD method treats the particles as the coarse-grained beads, whose motion is governed by the internal forces $\vec{f}^{\text{in}}$ resulting from the sum of the conservative force, dissipative force $\vec{f}^{\text{D}}$, and random force $\vec{f}^{\text{R}}$. The block copolymers are modelled as linked beads connected by the finite extensible nonlinear elasticity (FENE) potential.[35] An external force $\vec{f}^{\text{ext}}$ along the *x*-axis direction is exerted on solvent particles constantly after equilibrium time of 6×10^3 time steps ($t = 180\tau$) as a driving force of vesicles.[36] The time unit τ in our simulation is expressed as $\tau = \left(mr_c^2/k_BT\right)^{1/2}$, where the mass of the particle m, the energy scale k_BT and cutoff radius r_c all take the value of 1. Here, k_B and T are the Boltzmann constant and system temperature, respectively. The dimensionless shear rate is denoted as $\dot{\gamma}^*$, which can reflect the magnitude of shear stress and facilitate comparisons with other works.[37,38] The detailed processes of the transformation from $\vec{f}^{\text{ext}}$ to $\dot{\gamma}^*$ can be derived according to our previous work.[39] Generally, $\dot{\gamma}^* = \bar{\dot{\gamma}}t_0$ is used for the calculation of $\dot{\gamma}^*$. The $\bar{\dot{\gamma}}$ and t_0 are the average shear rate and the vesicle relaxation characteristic, respectively. $\bar{\dot{\gamma}}$ can be calculated by $\bar{\dot{\gamma}} = \bar{v}/D_T$. $\bar{v}$ and D_T are the average fluidic flow velocity and the diameter of the channel, respectively. t_0 is the characteristic parameter related to relaxing to a new steady state.[40] It is obtained from the formula $\tau_0 = \eta D_V^3/k_r$, where D_V, k_r and η are the diameters of the vesicle, the bending rigidity and the fluid dynamical viscosity of vesicle membrane, respectively.[37] The details about the k_r and η are provided in the electronic supplementary information (ESI).

The fluid environment consists of a confined channel flow and a single vesicle, and the profile of the flow basically satisfies $v_x/\bar{v} = 2(1 - r^2/R^2)$, which can refer to our previous work.[39] The initial vesicle consists of A_2B_4 amphiphilic block copolymers where beads A and B are hydrophilic and hydrophobic, respectively. It is formed during the time steps of 2×10^6 in selective solvent in a cubic box (20^3) under the periodic boundary conditions. The polymer centration is 0.1. The number density of the system is set to be 3. The interactions between DPD particles take the values of $a_{ii} = 25$ (i = A, B, or S), $a_{AB} = 85$, $a_{BS} = 110$, and $a_{AS} = 25$. We further measure the center of mass and the radius of the initial vesicle for determining geometric parameters of the channel.

We define the confinement degree C_d as $C_d = D_V/D_T$, which can reflect the size of the channel diameter with respect to the diameter of the vesicle. An equilibrated initial vesicle with the diameter of 11.02 prepared is placed into the center of the channel of length L_x=60. The channel satisfies periodic boundary condition along *x*-axis direction (flow direction) and a specular reflection boundary is employed at the wall of the channel.[41] The ratio of viscosity λ equals 1 due to the same particles inside and outside the vesicles. Matching viscosity (λ=1) is usually adopted in the experiment.[42] The density ρ of particles is set as 3. The interaction parameters between different kinds of particles are same with the system of initial formed vesicle. Each simulation takes the time exceeding $9\times10^4\tau$.

RESULTS AND DISCUSSION

Morphological Diagram Formed by Vesicles in the Flow

Systematic scan of morphologies has been performed in the parameter space ($\dot{\gamma}^*$, C_d) at t=9×10^4 τ as shown in the morphological diagram of Fig. 1. We observed six morphologies: vesicles, bullet-like vesicles, leaking vesicles, hamburger-like micelles, bilayers, and sphere micelles. The different morphological regions are drawn with different colors for convenience of observation. The detailed information of morphologies can refer to our previous work.[39] The black line presents the boundary between the morphologies with the unimpaired membranes and the others that have experienced the leakage. Vesicles with no leakage occur when $\dot{\gamma}^*$<6. The grey and purple regions correspond to the morphologies of vesicles and bullet-like vesicles, respectively. The bullet-like vesicles are elongated morphologies with tapered heads and their values of asphericity parameters A exceed 0.1. This morphology was found in the experimental[43] and theoretical[44] studies of the vesicles and RBCs under the flow. The bullet-like vesicles occur with the larger C_d values (C_d=0.8 and 0.9). However, the shape of vesicle morphology near C_d=0.5 is nearly spherical due to weak deformation of morphologies as analyzed before.[39] The vesicles under weak confinement are difficult to undergo the deformation compared with the strong confinements. But the rotation motion can be discovered under weak confinement

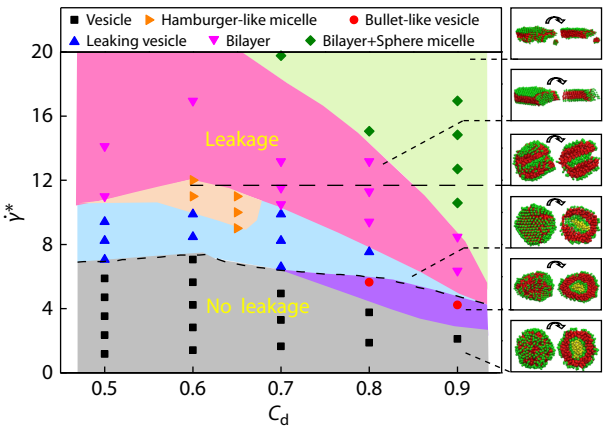

Fig. 1 The morphological diagram formed by vesicles in the flow for different values of $\dot{\gamma}^*$ and C_d at time t=9×10$^4\tau$. Different colors are used to mark the various morphologies. The snapshots of the morphologies are shown in the right. The morphologies in the phase regions below the black line do not experience the leakage.

according to the theory that the elongational behavior is not expected when it is the pure rotational flow.[45] Therefore, we mainly focus on the motion of the vesicle at C_d=0.5 in the following.

Movement of Particles on the Vesicle Membrane

The vesicles can exhibit different behavior of motion in the Poiseuille flow.[34] The two particles on the internal and external surfaces of the membrane are chosen as the markers to qualitatively reflect the relative motion of particles on the membrane as shown in Fig. 2. This method was usually used in the simulation[46] and experimental[18] research. The blue and yellow colors are used to label the particles on the internal (Fig. 2a) and external membrane (Fig. 2b), respectively. The moving of particles attached on the external membrane is also illustrated in Movie S1 (in ESI). Meanwhile, the sizes of the particles chosen are enlarged and the hydrophobic particles are not drawn in Fig. 2(a) for clarity. When t=240τ, particles with blue color are in the right corner of the inner cavity as viewed from the front of the vesicle. The two particles move with the increase in time, and two characteristic snapshots are presented at t=6360τ and 8580τ. The arrows show the direction of the motion of the two particles. These two particles in the vicinity of the edge at time of 8580τ move away from the left edge of inner cavity and enter the area at the back of the vesicle at t=12420τ. There is no significant change in their position along y-axis direction within the selected time. The two blue particles move with the same frequency in Fig. 2(a).

Furthermore, the similar phenomenon of the two yellow particles on the external surface of the membrane can be observed in Fig. 2(b). The positions of the selected particles on internal and external surface of the membrane are similar relative to the vesicles at the same time. One can conclude that the internal and external surfaces of the membrane move with the same frequency. Therefore, the characterization of motion frequency of the membrane can be approximately described by using a single particle. The motion of multiple particles on the membrane with same frequency was also found in the research of Fischer *et al.*[18] This motion performs like the rolling in the two dimensional research of the RBCs as referred by Tusch *et al.*[47] We further demonstrate the motion type in the next section. Furthermore, we infer that occurrence of this motion is related to membrane displacement caused by the off-center of vesicles.[37] Goldsmith *et al.* experimentally observed tumbling motion of single RBC with opposite rotation on opposite sides of a tube under the microscope in Poiseuille flow.[24]

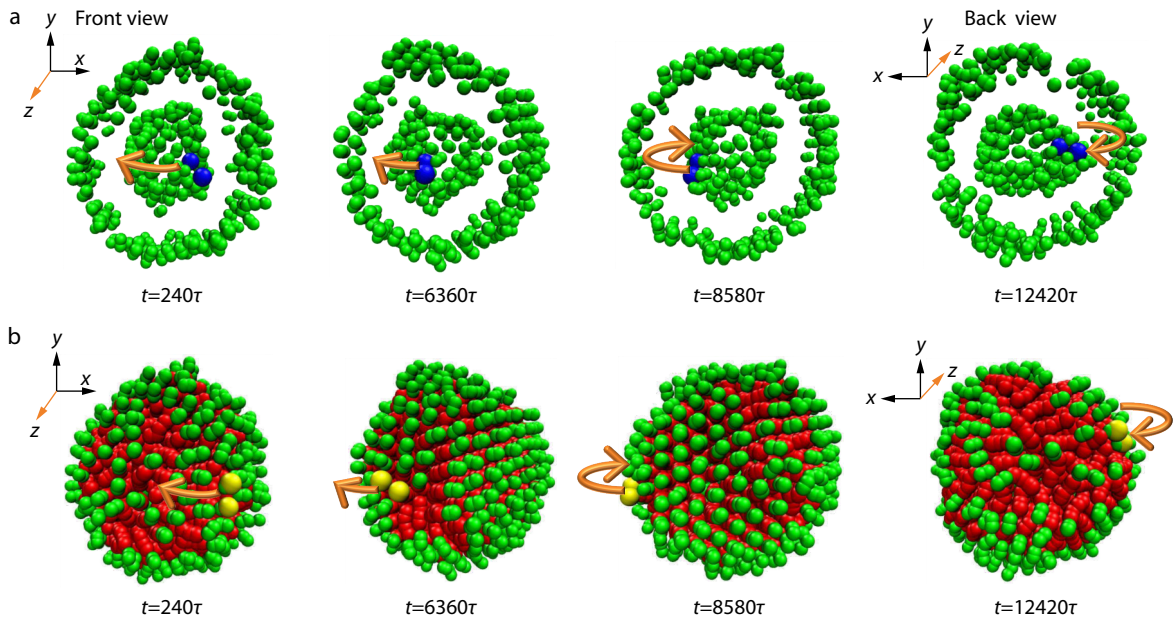

Fig. 2 Snapshots of vesicles with two attached blue (yellow) hydrophilic beads on the (a) inner hydrophilic layer and (b) outer hydrophilic layer of vesicle when $\dot{\gamma}^*$ = 5.88 and C_d = 0.5. Here, the coordinate axes in the left corners of the images correspond to the view of the observed vesicles and they are not labeled when the same view appears as in the left front image. Arrows mark the direction of bead motion. The fluorescent beads chosen are properly enlarged.

https://doi.org/10.1007/s10118-022-2774-5

Vesicle Movement with Unfixed Axes

Measurements of the motion axes were conducted in the Poiseuille flow *via* finding the almost motionless beads. It allows us to capture the motion characteristics. We exhibit the time-stacking of bead trajectories marked by different colors at different intervals of time when $\dot{\gamma}^* = 5.88$ and $C_d = 0.5$ in Fig. 3(a). The orange arrows reflect the directions of the rotation of the membrane and red beads are the hydrophobic particles of membranes. The highlighted beads around the vesicle are marked in different colors for distinguishing to visualize the membrane motion. The rotational axis and the direction meet the right-hand rule. The time interval between every two consecutive points on the trajectory is 60τ, and they are close packing of the consecutive points owing to slow paces for each time interval. Before the axes shift, the time- stacking of a certain bead is approximately a circle and it forms the vorticity trajectories like the "parallel". We can observe the orbits formed by the trajectories of beads over time are parallel to each other and they can maintain the stabilization of the relative position as stated above. These trajectories also occur at the surfaces of giant lipid vesicles immersed in a shear flow, as observed in the experiment of Vézy *et al.*[48] We classify this motion as rolling. Dupire *et al.* described the RBC rolling as the wheel on the road, and it steadily spins around the vorticity axis.[26] The occurrence of rolling motion in shear flow can induce less deformations by avoiding energetical cost. The full orbits are not observed because of the unsteady changes of the axes. The orbital variations are easy to be observed. Time intervals are determined by the state of the orbit. There are four time-intervals, corresponding to four orbits with different orientations formed by the particle trajectories. The orbit remains constant in the same interval. Due to the unfixed-orientations of the orbit over time, we consider the motion of membrane as the unsteady periodic rolling.

The trajectories of the beads near the axes of the membrane are also investigated in Fig. 3(b). Due to their positions in the close vicinity of two stagnation points, their trajectories exhibit circular rotations with small radii. Their location appears within a certain range, which is the trajectory characteristic of beads near the axes. The qualitative directions of the rotation axes of the membranes are also presented as the orange arrows. Their unit vectors $\vec{n}_1$ =(0.1219, −0.9270, 0.3546), $\vec{n}_2$ =(0.4437, −0.4454, −0.7776), $\vec{n}_3$ =(−0.1875, 0.1280, 0.9739), and $\vec{n}_4$ =(0.3682, −0.1018, 0.9242) along the axes can

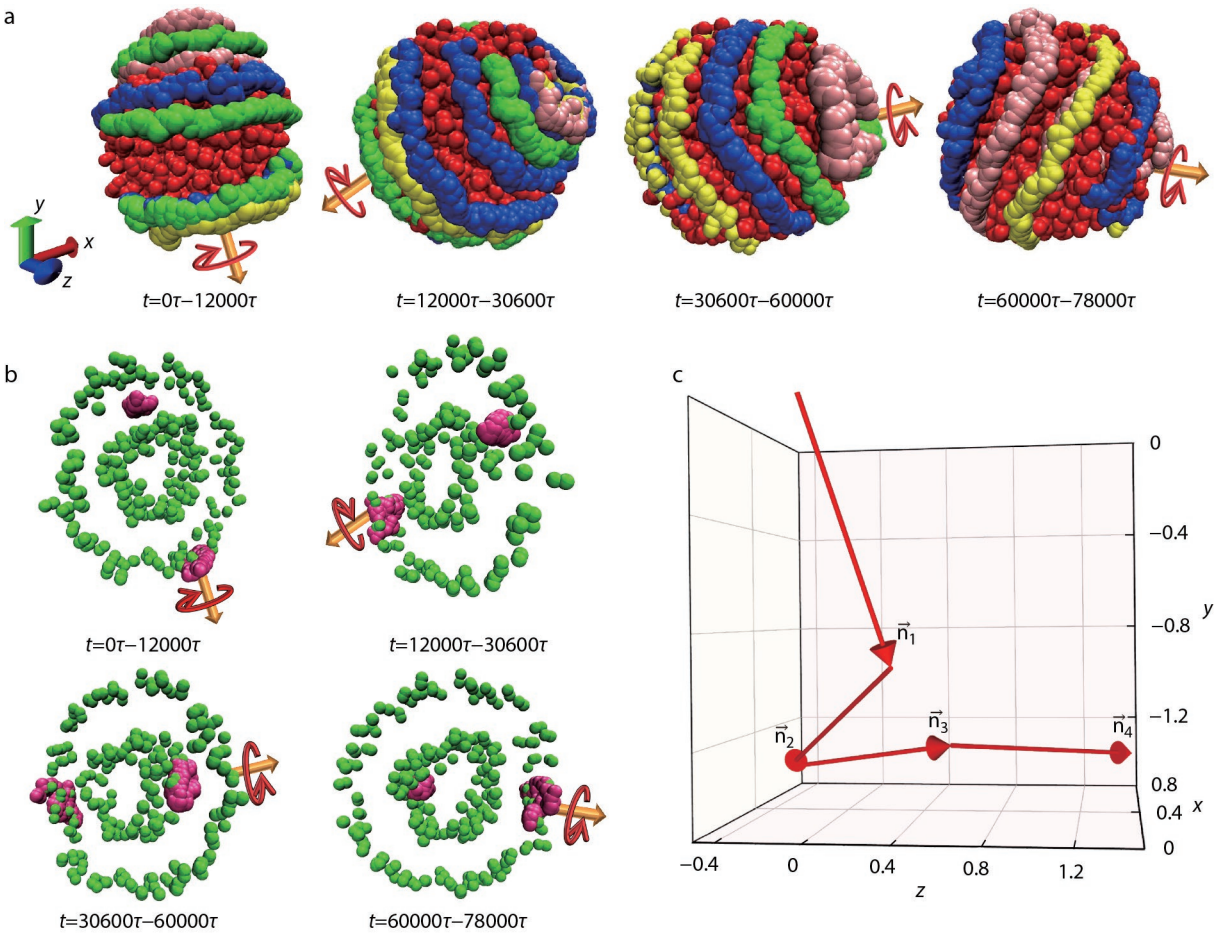

Fig. 3 (a) The time-stacking formed by trajectories of characteristic hydrophilic particles marked by the different colors outside the vesicle when $\dot{\gamma}^* = 5.88$ and $C_d = 0.5$ at different intervals of time. Here, the same view is chosen as in the lower left image. The red and orange arrows present the directions of the rotation and axes; (b) Time-stacking of the beads chosen near the axis are marked by the pink color; (c) The unit vectors of axes at different time: $\vec{n}_1$ =(0.1219, −0.9270, 0.3546), $\vec{n}_2$ = (0.4437, −0.4454, −0.7776), $\vec{n}_3$ =(−0.1875, 0.1280, 0.9739), $\vec{n}_4$ =(0.3682, −0.1018, 0.9242).

https://doi.org/10.1007/s10118-022-2774-5

be obtained according to the two dots on the axes, which are drawn in the Cartesian coordinate system of Fig. 3(c) for intuitive observation. The orientational angles between the unit vectors including $\vec{n}_1$ to $\vec{n}_4$ and the *yz* plane are approximately 7°, 26.4°, 10.8°, and 21.6°, respectively. We can see the four vectors are nearly parallel with the *yz* plane in Fig. 3(c). This indicates the *x*-axis and orbits of trajectories formed by the beads on the membrane of the vesicles with time are parallel because the unit vectors is perpendicular to the orbit plane. The axis for motion is unfixed with the increase of time in our work. Fedosov *et al.* also reported the unfixed axes of tumbling, the shift of orbits, and oscillations along the vorticity direction in the study of RBCs under the tube flow.[37]

Rolling Orientation of Vesicles

In this part, we focus on the deviation of the particles on the vesicle from the *x*-axis caused by the flow, and thus the orientations with respective to the *x*-axis are discussed. We define that the vector $\vec{r}$ is from the mass center of the vesicle to particles and distance *r* can be expressed as $r=|\vec{r}|$. θ is the angle between the vector $\vec{r}$ and the positive direction of *x*-axis as shown in Fig. 4(a). The dynamic evolution behaviors in *x*-axis direction and its orthogonal direction are considered. We mainly discuss the velocity of motion of particles with respective to the *x*-axis. Usually, the particles on the equator are chosen to describe the movement of the membrane (Fig. 4b). Fig. 4(c) presents the evolution of the angles θ and distance r^2 using the particle (the yellow bead in Fig. 4b) on the internal membrane of the vesicles, respectively. They have the similar trend. The red arrows point the peaks of the distributions. The first and second peaks occur near $t=1.5\times10^4\tau$ and $t=5.3\times10^4\tau$ for both θ and r^2. This characteristic is similar to the tank-treading. There are changes of distance *r* when vesicles move in the mode of tank-treading but no change in the tumbling. The similar results are also found in particle (the blue bead in Fig. 4b) on the external surface of membrane shown as the Fig. 4(d).

The above analysis shows that we can detect the temporal evolution of angles of movement with respect to the flow direction using particles near the equatorial region. The measurements of θ by choosing a single particle at proximity of central trajectories were carried out for $\dot{\gamma}^*=5.88$, 4.71, 3.53, and 2.35 with a fixed $C_d=0.5$ when $t=0-1.8\times10^5\tau$ as shown in Fig. 5. Due to the changes of axes, different particles are chosen as the markers. The successive changes of angles over time can be observed as muti-periodic and stable rolling from Fig. 5(a) to Fig. 5(c). We observe the similar tendency of the angle variation before and after changes of the axes. Their angles vary from 0 to 3.14 (radian). The period of the rolling increases with the decrease of $\dot{\gamma}^*$. We observe the decrease of θ over time and then its value tends to zero with small fluctuations after $t=27077\tau$ when $\dot{\gamma}^*=2.35$ shown as Fig. 5(d). It is not sufficient to drive the rolling motion for the stress exerted by the flow with a weaker $\dot{\gamma}^*$ as previously reported.[23,26] The vesicles become the "fluidization" from the solid-like state by overcoming the energy barrier.[26] This implies the critical value of $\dot{\gamma}^*$reaching "fluidization" of membranes is between 2.35 and 3.53.

The temporal evolution of θ under $C_d=0.8$ shown in Fig. 6 is detected to reflect the dependence of θ on the confinement degrees to compare with Fig. 5. At the initial state, their particle markers start from the same value of θ, and the corresponding position is pointed by an orange arrow in the illustration of Fig. 6. In these cases, the θ reaches steady-state

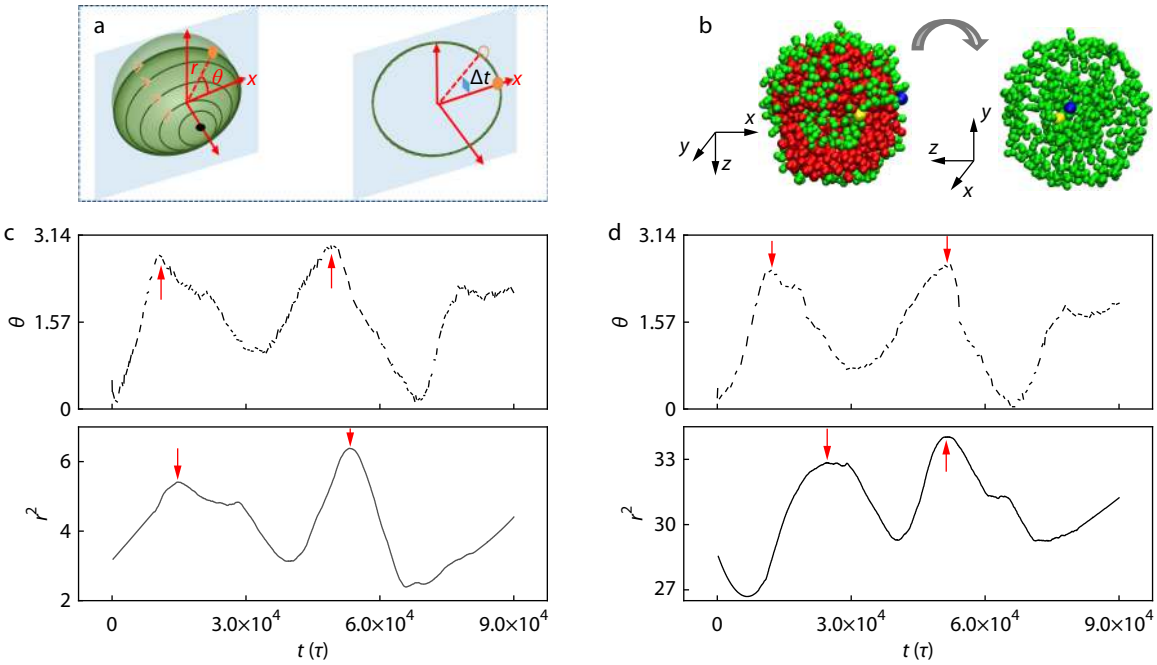

Fig. 4 (a) The schematic model to define the orientation angle θ and distance *r* from the center of the vesicle; (b) The particles chosen on the vesicles are marked as blue and yellow at $t=0$ and arrows point to them. The left snapshot is in the front view and the right one is in the right view. The sizes of particles chosen are enlarged for clarity. One-quarter of the vesicle is cut away in left snapshot and the hydrophobic beads are not shown in the right one. The θ and r^2 of hydrophilic particles inside (c) and outside (d) the vesicle as functions of time when $\dot{\gamma}^*=5.88$ and $C_d=0.5$.

https://doi.org/10.1007/s10118-022-2774-5

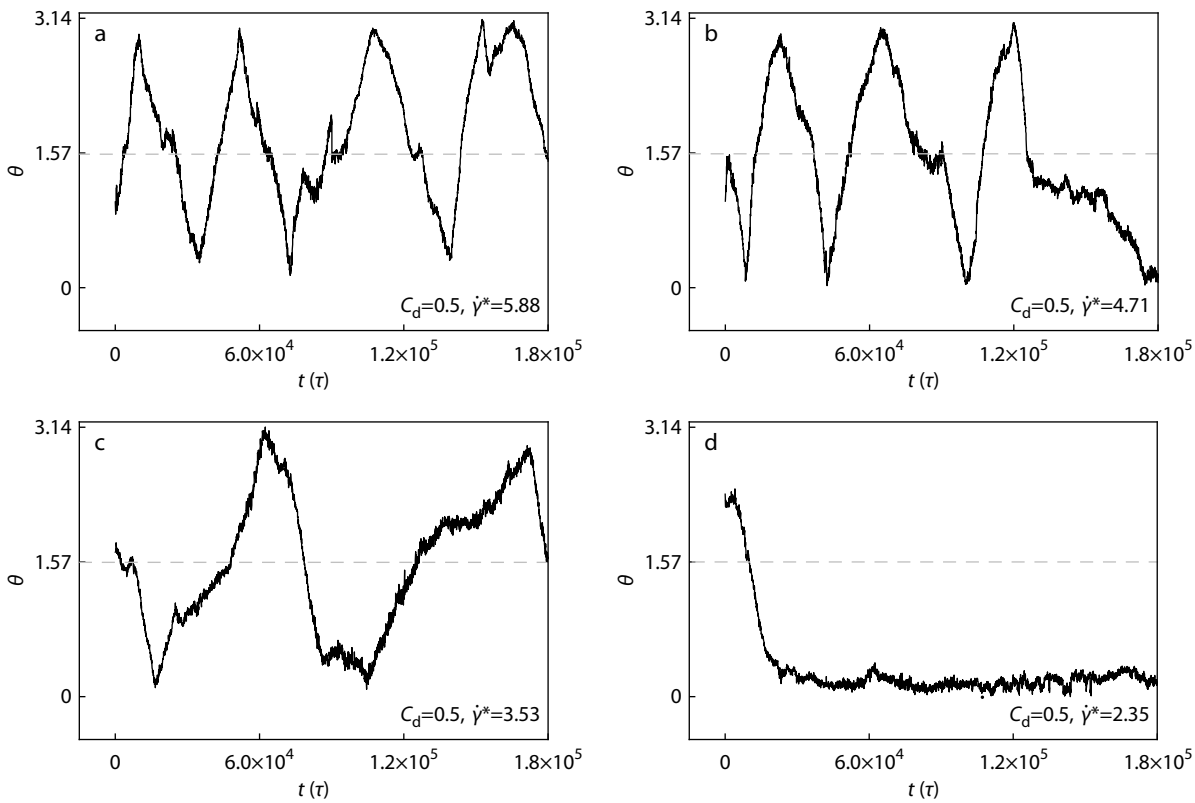

Fig. 5 Time evolution of θ for (a) $\dot{\gamma}^*=5.88$, (b) $\dot{\gamma}^*=4.71$, (c) $\dot{\gamma}^*=3.53$, and (d) $\dot{\gamma}^*=2.35$ with a fixed $C_d=0.5$ at $t=0\tau-1.8\times10^5\tau$. Here, particles chosen are different due to axis change in the same parameter.

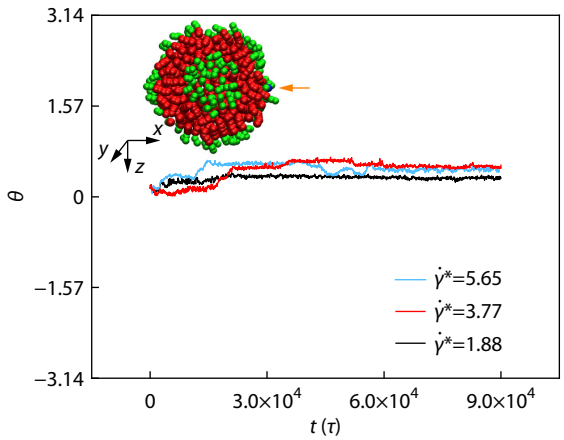

Fig. 6 Time evolution of the orientation of θ when $\dot{\gamma}^*=5.65$, 3.77 and 1.88 with fixed $C_d=0.8$ at $t=0\tau-9\times10^4\tau$. The illustration is the section of an initial vesicle with an orange arrow pointing to a blue marker, which is used in the measurement of θ in the three cases.

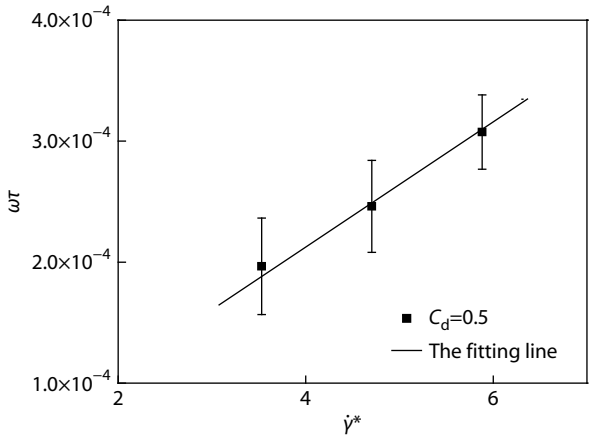

Fig. 7 The angular velocity $\omega\tau$ of a circulating marker on the membrane of the vesicle as functions of $\dot{\gamma}^*$ when $C_d=0.5$. The line is fitted.

values after slight increases. The increases of θ occur when the deformation degree of vesicles is small at the beginning of the tests. Rolling is hardly observed for the whole period of time. Less change in θ occurs as compared to the C_d value of 0.5. This indicates the rolling of vesicle is difficult at the higher C_d and the vesicles require more energy for obtaining rolling. In other words, the strong confinement weakens the rolling. However, the significant change of vesicles induced by the flow is the shape transformation according to Fig. 1 when the magnitude of the C_d is relatively large, *i.e.*, C_d = 0.8. It is consistent with the results of Kaoui *et al.*[32]

Overall Motion of the Vesicle

The dimensionless angular velocity $\omega\tau$ is calculated based on the data of Fig. 5. Time intervals when large fluctuations occur are not considered. According to Figs. 5(a)–5(c), we chose 10, 10, and 13 time-interval samples for statistics, respectively. The relationship between $\omega\tau$ and $\dot{\gamma}^*$ is displayed in Fig. 7. ω is computed using the equation $\omega = \Delta\theta/\Delta t$, which is used to describe the behaviors of motion.[11,37,48] The $\omega\tau$ can be

measured using the trajectories located on the vesicles.[48] Here, the choice of trajectories rarely influences the results due to their same frequency as stated above. The fitting line is drawn as a solid line. The extension of the line can pass through the coordinate origin. The values of $\omega\tau$ can characterize the velocity of the rolling and increase linearly upon increasing $\dot{\gamma}^*$, implying the positive dependence of $\omega\tau$ on $\dot{\gamma}^*$. Meanwhile, the slope of the line in Fig. 7 is small compared to the results in tumbling and tank-treading in shear flow because of the small gradient of velocity induced by the lateral excursion of the center of mass in Poiseuille flow, which will be discussed in the next paragraph.

The intricate behaviors of the vesicle also include the vertical position change of the mass center of the vesicle with respective to the flow direction in the Poiseuille flow.[37,49] It can characterize the amplitude of the snaking. In Fig. 8, the excursion of position of the mass center with respective to the centerline in three-dimension parameter space (t/τ, y/R_v, z/R_v) is shown when $\dot{\gamma}^*=5.88$, 4.71, 3.53 and 2.35 with a fixed C_d value of 0.5. Here, R_v is the radius of the vesicle. The blue line is along the centerline of the channel. The curves formed

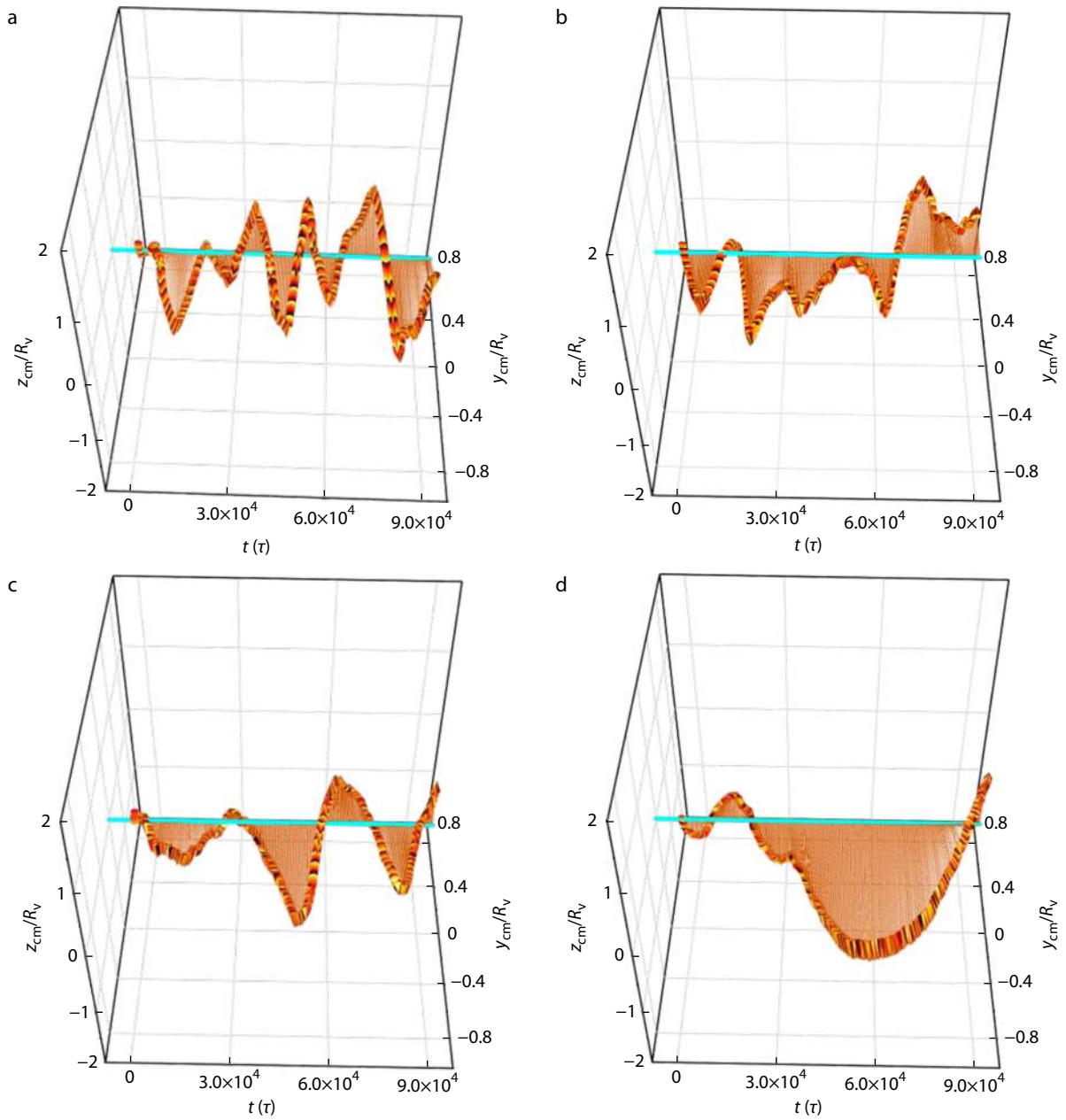

Fig. 8 The lateral excursion of the center of mass in the *yz* plane as a function of time when (a) $\dot{\gamma}^*=5.88$, (b) $\dot{\gamma}^*=4.71$, (c) $\dot{\gamma}^*=3.53$, and (d) $\dot{\gamma}^*=2.35$ with a fixed C_d value of 0.5. y_{cm} and z_{cm} are the distances between the center of mass of the vesicles and the centerline of channel along *y*- and *z*-axis direction, respectively. R_v is the radius of the vesicle. The blue line is the centerline of the channel. The thick curves are formed by the trajectories of mass centers over time and the orange thin lines form by connecting the centerline of channel and temporal mass center.

https://doi.org/10.1007/s10118-022-2774-5

by the position of the center of mass present a spiral zigzagging around the centerline of the channel. We can observe the complex state with multi-periodic oscillations. By reducing $\dot{\gamma}^*$, we can obtain larger period of the oscillation and lower frequency. But the period and the amplitude of the oscillations are irregular. Similarly, Aouane *et al*. presented the unstable motion with off-centered snaking when the confinements are weaker than the critical confinements.[34] We can observe centered and off-centered snaking in our simulation, which have the characteristics of symmetrical and asymmetrical lateral excursion of the center of mass over a oscillation period, respectively.[49] The amplitude of y_{cm}/R_v basically remains unchanged with the increase in $\dot{\gamma}^*$ as shown in Fig. S1 (in ESI). The motion of vesicle in the shear flow is usually attributed to the velocity gradient. We find reversal oscillations of the vesicle around the centerline of the channel are related to the axis change by comparing Fig. 3 and Fig. S1(a) (in ESI). The values of time when the axes change are 12000τ, 30600τ, 60000τ, and 78000τ in Fig. 3(a). At these time points, turning points occur in Fig. S1(a) (in ESI), owing to the variations of directions of shear in 3D space. In the case of $\dot{\gamma}^*=5.88$, 4.71, 3.53 and 2.35, and fixed $C_d=0.5$, the asphericity A varies with time in the range of 0−0.005 as shown in Fig. S2 (in ESI). The shapes of vesicles are approximately spherical over the simulation time in these situations. The directional changes of shear induced by the vesicle rotation and lateral excursion are helpful for the vesicle to avoid being constantly elongated in a single direction. Hence, there are oscillation changes of A values in Fig. S2 (in ESI). The different C_d can affect the lateral motion behaviors, as shown in Fig. S3 (in ESI). It presents the excursion of the center of mass in the y-axis and z-axis direction as a function of time when $\dot{\gamma}^*=5.65$, $\dot{\gamma}^*=3.77$, and $\dot{\gamma}^*=1.88$ with a fixed C_d value of 0.8. There is no obvious position variation in the yz plane as compared to Fig. 8. Because the shape of the initial vesicle and its position in the plane (y, z) of the channel are symmetric, the symmetry of pressure around the vesicle is not broken leading to the absence of the rolling as shown in Fig. 6.

CONCLUSIONS

In summary, we utilized the DPD method to explore the dynamic behaviors of vesicles suspended in the confined Poiseuille flow by tuning the parameters including the dimensionless shear rates and the confinement degrees. The morphological diagram formed by vesicles at given time as a function of dimensionless shear rate and confinement degrees is constructed. The motion of vesicles induced by the flow is identified as the rolling by judging the trajectory of particle markers attached on the membrane. However, the axes of rolling unsteadily change with time. We also examined the dependence of rolling angle evolution on the confinement degrees or dimensionless shear rates. It is based on the same frequency of motion of particles on the membrane of vesicles. The results show that the strong confinement degree constrains the occurrence of the rolling. Vesicles under smaller shear rates have the lower frequency of the rolling and the slower angular velocity of the rolling. Finally, we propose a possible interpretation of the unfixed axes by measuring the lateral excursions for different dimensionless shear rates. Therefore, we can describe the motion of vesicles as the complicated and unsteady 3D rolling around the unfixed axes.

NOTES

The authors declare no competing financial interest.

Electronic Supplementary Information

Electronic supplementary information (ESI) is available free of charge in the online version of this article at http://doi.org/10.1007/s10118-022-2774-5.

ACKNOWLEDGMENTS

This work was financially supported by the National Natural Science Foundation of China (Nos. 21973041, 22173045, 21973040, 21674047 and 21734005), the Program for Changjiang Scholars and Innovative Research Team in University (PCSIRT) and the Fundamental Research Funds for the Central Universities. The numerical calculations have been done on the IBM Blade cluster system in the High Performance Computing Center (HPCC) of Nanjing University.

REFERENCES

1 Holm, S. H.; Beech, J. P.; Barrett, M. P.; Tegenfeldt, J. O. Separation of parasites from human blood using deterministic lateral displacement. *Lab Chip* **2011**, *11*, 1326–1332.
2 Krüger, T.; Holmes, D.; Coveney, P. V. Deformability-based red blood cell separation in deterministic lateral displacement devices—a simulation study. *Biomicrofluidics* **2014**, *8*, 054114.
3 Davis, J. A.; Inglis, D. W.; Morton, K. J.; Lawrence, D. A.; Huang, L. R.; Chou, S. Y.; Sturm, J. C.; Austin, R. H. Deterministic hydrodynamics: taking blood apart. *Proc. Natl. Acad. Sci. U. S. A.* **2006**, *103*, 14779–14784.
4 Zare, R. N.; Kim, S. Microfluidic platforms for single-cell analysis. *Annu. Rev. Biomed. Eng.* **2010**, *12*, 187–201.
5 Yin, H.; Marshall, D. Microfluidics for single cell analysis. *Curr. Opin. Biotechnol.* **2012**, *23*, 110–119.
6 Holme, M. N.; Fedotenko, I. A.; Abegg, D.; Althaus, J.; Babel, L.; Favarger, F.; Reiter, R.; Tanasescu, R.; Zaffalon, P. L.; Ziegler, A. Shear-stress sensitive lenticular vesicles for targeted drug delivery. *Nat. Nanotechnol.* **2012**, *7*, 536–543.
7 Saxer, T.; Zumbuehl, A.; Müller, B. The use of shear stress for targeted drug delivery. *Cardiovasc. Res.* **2013**, *99*, 328–333.
8 Henry, E.; Holm, S. H.; Zhang, Z.; Beech, J. P.; Tegenfeldt, J. O.; Fedosov, D. A.; Gompper, G. Sorting cells by their dynamical properties. *Sci. Rep.* **2016**, *6*, 1–11.
9 Merola, F.; Memmolo, P.; Miccio, L.; Savoia, R.; Mugnano, M.; Fontana, A.; D'ippolito, G.; Sardo, A.; Iolascon, A.; Gambale, A. Tomographic flow cytometry by digital holography. *Light: Sci. Appl.* **2017**, *6*, e16241.
10 Noguchi, H.; Gompper, G. Fluid vesicles with viscous membranes in shear flow. *Phys. Rev. Lett.* **2004**, *93*, 258102.
11 Noguchi, H.; Gompper, G. Dynamics of fluid vesicles in shear flow: effect of membrane viscosity and thermal fluctuations. *Phys. Rev. E* **2005**, *72*, 011901.
12 Noguchi, H.; Gompper, G. Swinging and tumbling of fluid vesicles in shear flow. *Phys. Rev. Lett.* **2007**, *98*, 128103.
13 Pozrikidis, C. Finite deformation of liquid capsules enclosed by

elastic membranes in simple shear flow. *J. Fluid Mech.* **1995**, *297*, 123–152.
14 Pozrikidis, C. Numerical simulation of the flow-induced deformation of red blood cells. *Ann. Biomed. Eng.* **2003**, *31*, 1194–1205.
15 Ramanujan, S.; Pozrikidis, C. Deformation of liquid capsules enclosed by elastic membranes in simple shear flow: large deformations and the effect of fluid viscosities. *J. Fluid Mech.* **1998**, *361*, 117–143.
16 Noguchi, H.; Gompper, G. Shape transitions of fluid vesicles and red blood cells in capillary flows. *Proc. Natl. Acad. Sci. U. S. A.* **2005**, *102*, 14159–14164.
17 Schmid-Schönbein, H.; Wells, R. Fluid drop-like transition of erythrocytes under shear. *Science* **1969**, *165*, 288–291.
18 Fischer, T. M.; Stohr-Lissen, M.; Schmid-Schonbein, H. The red cell as a fluid droplet: tank tread-like motion of the human erythrocyte membrane in shear flow. *Science* **1978**, *202*, 894–896.
19 Fischer, T. M. Tank-tread frequency of the red cell membrane: dependence on the viscosity of the suspending medium. *Biophys. J.* **2007**, *93*, 2553–2561.
20 Barthes-Biesel, D.; Rallison, J. The time-dependent deformation of a capsule freely suspended in a linear shear flow. *J. Fluid Mech.* **1981**, *113*, 251–267.
21 Keller, S. R.; Skalak, R. Motion of a tank-treading ellipsoidal particle in a shear flow. *J. Fluid Mech.* **1982**, *120*, 27–47.
22 Misbah, C. Vacillating breathing and tumbling of vesicles under shear flow. *Phys. Rev. Lett.* **2006**, *96*, 028104.
23 Skotheim, J.; Secomb, T. W. Red blood cells and other nonspherical capsules in shear flow: oscillatory dynamics and the tank-treading-to-tumbling transition. *Phys. Rev. Lett.* **2007**, *98*, 078301.
24 Goldsmith, H.; Marlow, J.; MacIntosh, F. C. Flow behaviour of erythrocytes-i. rotation and deformation in dilute suspensions. *Proc. R. Soc. London, Ser. B* **1972**, *182*, 351–384.
25 Abkarian, M.; Faivre, M.; Viallat, A. Swinging of red blood cells under shear flow. *Phys. Rev. Lett.* **2007**, *98*, 188302.
26 Dupire, J.; Socol, M.; Viallat, A. Full dynamics of a red blood cell in shear flow. *Proc. Natl. Acad. Sci. U. S. A.* **2012**, *109*, 20808–20813.
27 Dupire, J.; Abkarian, M.; Viallat, A. Chaotic dynamics of red blood cells in a sinusoidal flow. *Phys. Rev. Lett.* **2010**, *104*, 168101.
28 Zhao, H.; Shaqfeh, E. S. The dynamics of a vesicle in simple shear flow. *J. Fluid Mech.* **2011**, *674*, 578–604.
29 Beaucourt, J.; Rioual, F.; Séon, T.; Biben, T.; Misbah, C. Steady to unsteady dynamics of a vesicle in a flow. *Phys. Rev. E* **2004**, *69*, 011906.
30 Junot, G.; Figueroa-Morales, N.; Darnige, T.; Lindner, A.; Soto, R.; Auradou, H.; Clément, E. Swimming bacteria in poiseuille flow: the quest for active Bretherton-Jeffery trajectories. *Europhys. Lett.* **2019**, *126*, 44003.
31 Deschamps, J.; Kantsler, V.; Steinberg, V. Phase diagram of single vesicle dynamical states in shear flow. *Phys. Rev. Lett.* **2009**, *102*, 118105.
32 Kaoui, B.; Krüger, T.; Harting, J. How does confinement affect the dynamics of viscous vesicles and red blood cells. *Soft Matter* **2012**, *8*, 9246–9252.
33 Kaoui, B.; Harting, J.; Misbah, C. Two-dimensional vesicle dynamics under shear flow: effect of confinement. *Phys. Rev. E* **2011**, *83*, 066319.
34 Aouane, O.; Thiébaud, M.; Benyoussef, A.; Wagner, C.; Misbah, C. Vesicle dynamics in a confined poiseuille flow: from steady state to chaos. *Phys. Rev. E* **2014**, *90*, 033011.
35 Kröger, M.; Hess, S. Rheological evidence for a dynamical crossover in polymer melts *via* nonequilibrium molecular dynamics. *Phys. Rev. Lett.* **2000**, *85*, 1128.
36 Chu, X.; Yu, X.; Greenstein, J.; Aydin, F.; Uppaladadium, G.; Dutt, M. Flow-induced shape reconfiguration, phase separation, and rupture of bio-inspired vesicles. *ACS Nano* **2017**, *11*, 6661–6671.
37 Fedosov, D. A.; Peltomäki, M.; Gompper, G. Deformation and dynamics of red blood cells in flow through cylindrical microchannels. *Soft Matter* **2014**, *10*, 4258–4267.
38 Reichel, F.; Mauer, J.; Nawaz, A. A.; Gompper, G.; Guck, J.; Fedosov, D. A. High-throughput microfluidic characterization of erythrocyte shapes and mechanical variability. *Biophys. J.* **2019**, *117*, 14–24.
39 Liu, D.; Zhang, Z.; Wang, R.; Hu, J. Stability and deformation of vesicles in a cylindrical flow. *Langmuir* **2022**, *38*, 629–637.
40 Barlow, B. M.; Bertrand, M.; Joós, B. Relaxation of a simulated lipid bilayer vesicle compressed by an atomic force microscope. *Phys. Rev. E* **2016**, *94*, 052408.
41 Visser, D.; Hoefsloot, H.; Iedema, P. Comprehensive boundary method for solid walls in dissipative particle dynamics. *J. Comput. Phys.* **2005**, *205*, 626–639.
42 Narsimhan, V.; Spann, A. P.; Shaqfeh, E. S. Pearling, wrinkling, and buckling of vesicles in elongational flows. *J. Fluid Mech.* **2015**, *777*, 1–26.
43 Coupier, G.; Farutin, A.; Minetti, C.; Podgorski, T.; Misbah, C. Shape diagram of vesicles in poiseuille flow. *Phys. Rev. Lett.* **2012**, *108*, 178106.
44 Danker, G.; Vlahovska, P. M.; Misbah, C. Vesicles in poiseuille flow. *Phys. Rev. Lett.* **2009**, *102*, 148102.
45 Smith, D. E.; Babcock, H. P.; Chu, S. Single-polymer dynamics in steady shear flow. *Science* **1999**, *283*, 1724–1727.
46 Kaoui, B.; Harting, J. Two-dimensional lattice boltzmann simulations of vesicles with viscosity contrast. *Rheologica Acta* **2016**, *55*, 465–475.
47 Tusch, S.; Loiseau, E.; Al-Halifa, A. H.; Khelloufi, K.; Helfer, E.; Viallat, A. When giant vesicles mimic red blood cell dynamics: swinging of two-phase vesicles in shear flow. *Phys. Rev. Fluids* **2018**, *3*, 123605.
48 Vézy, C.; Massiera, G.; Viallat, A. Adhesion induced non-planar and asynchronous flow of a giant vesicle membrane in an external shear flow. *Soft Matter* **2007**, *3*, 844–851.
49 Kaoui, B.; Tahiri, N.; Biben, T.; Ez-Zahraouy, H.; Benyoussef, A.; Biros, G.; Misbah, C. Complexity of vesicle microcirculation. *Phys. Rev. E* **2011**, *84*, 041906.

https://doi.org/10.1007/s10118-022-2774-5